A&A 652, A29 (2021)
https://doi.org/10.1051/0004-6361/202140579

Astronomy & Astrophysics

Ammonia snow lines and ammonium salts desorption

F. Kruczkiewicz[1,2,3], J. Vitorino[2], E. Congiu[2], P. Theulé[1], and F. Dulieu[2]

[1] Aix Marseille Univ, CNRS, CNES, LAM, Marseille, France
e-mail: fkrucz@mpe.mpg.de
[2] CY Cergy Paris Université, Observatoire de Paris, PSL University, Sorbonne Université, CNRS, LERMA, 95000 Cergy, France
[3] Max-Planck-Institut für extraterrestrische Physik, Gießenbachstraße 1, Garching, 85748, Germany

Received 16 February 2021 / Accepted 16 April 2021

ABSTRACT

Context. The nitrogen reservoir in planetary systems is a long-standing problem. Some of the N-bearing molecules are probably incorporated into the ice bulk during the cold phases of the stellar evolution, and may be gradually released into the gas phase when the ice is heated, for example in active comets. The chemical nature of the N-reservoir should greatly influence how, when, and in what form N returns to the gas phase, or is incorporated into the refractory material forming planetary bodies.
Aims. We present the study of the thermal desorption of two ammonium salts, ammonium formate and ammonium acetate, from a gold surface and from a water ice substrate.
Methods. Temperature-programmed desorption experiments and Fourier transform infrared reflection spectroscopy were conducted to investigate the desorption behavior of ammonium salts.
Results. Ammonium salts are semi-volatile species releasing neutral species as major components upon desorption, namely ammonia and the corresponding organic acid (HCOOH and CH_3COOH), at temperatures higher than the temperature of thermal desorption of water ice. Their desorption follows a first-order Wigner-Polanyi law. We find the first-order kinetic parameters $A = 7.7 \pm 0.6 \times 10^{15}$ s^{-1} and $E_{\rm bind} = 68.9 \pm 0.1$ kJ mol^{-1} for ammonium formate and $A = 3.0 \pm 0.4 \times 10^{20}$ s^{-1} and $E_{\rm bind} = 83.0 \pm 0.2$ kJ mol^{-1} for ammonium acetate. The presence of a water ice substrate does not influence the desorption kinetics. Ammonia molecules locked in salts desorb as neutral molecules at temperatures much higher than previously expected, and that are usually attributed to refractory materials.
Conclusions. The ammonia snow line has a smaller radius than the water snow line. As a result, the NH_3/H_2O ratio content in Solar System bodies can be a hint to where they formed and subsequently migrated.

Key words. astrochemistry – molecular processes – methods: laboratory: solid state – ISM: molecules – protoplanetary disks – comets: general

1. Introduction

The abundance of nitrogen, the fifth most abundant element in the Universe, has always been a matter of debate (Maiolino & Mannucci 2019), in the extra-galactic interstellar medium (ISM) and in the local ISM, because nitrogen has both a primary and a secondary nucleosynthetic contribution (Vila-Costas & Edmunds 1993), and because nitrogen has a significant depletion factor of 0.89 (Savage & Sembach 1996) indicating that a fraction of nitrogen has been incorporated into dust grains (mainly as titanium nitride, TiN). In the Solar System as well, the N abundance is among the more uncertain elemental abundances (Lodders 2010); it has been estimated to be 7.24×10^{-5} with respect to hydrogen (Caffau et al. 2009; Grevesse et al. 2010). Nitrogen can have several carriers, depending on the phase of the ISM. In the diffuse ISM, nitrogen is mostly atomic in its neutral or ionized form; the column densities derived from vacuum ultraviolet (VUV) and UV absorption lines of molecular nitrogen (Knauth et al. 2004) is several orders of magnitude lower than that of atomic nitrogen (Nieva & Przybilla 2012). In dense clouds, although neutral nitrogen (NI) and molecular nitrogen (N_2) are not observable directly, indirect observations using diazenylium (N_2H^+; Maret et al. 2006) lead to the conclusion that atomic nitrogen is the dominant reservoir of nitrogen.

Other N-bearing molecules such as NO, CN, NS, and NH diatomic radicals, or NH_3, HCN, HNCO, HNC, and N_2H^+ are observed with variable abundances in different sources (Omont 2007), NH_3 being the most abundant of the gas-phase carrier at a typical abundance of a few 10^{-8} with respect to molecular hydrogen. In pre-stellar cores it is likely that nitrogen is incorporated into the dust grain icy mantles. A recent study by Punanova et al. (2018) illustrates this specific property and demonstrates how N-bearing molecules can map the densest parts of star-forming regions such as filaments in the Taurus molecular cloud. The hyper-fine structure of ortho-NH_3 (1_0–0_0) has been resolved for the first time in space (Caselli et al. 2017) by observing a dark molecular cloud, confirming previous estimates of dynamics and abundances. The chemical model developed underestimates the abundance of NH_3 toward the center of the nucleus by more than an order of magnitude, and overestimates its abundance by about two orders of magnitude in the outer regions (Hily-Blant et al. 2010). The Spitzer ice survey showed that in star-forming regions the most abundant N-bearing ices are NH_3, NH_4^+, and OCN^-, with typical abundances (but with large uncertainties) of about 4×10^{-6}, 4×10^{-6}, and 4×10^{-7} with respect to hydrogen nuclei, respectively (Boogert et al. 2015), HCN being undetected in interstellar ices. However, these three main N-carriers only account for about 10% of the overall nitrogen elemental budget (Öberg et al. 2011). The missing N may be partially found as N_2, but it is almost undetectable in this form (Boogert et al. 2015). In young stellar objects and outflows, where the ice is sublimated by radiative or shock heating (Riaz et al. 2018;

Tafalla et al. 2010), the abundances of N-bearing molecules increase but still cannot account for the initial atomic abundances. In the Solar System, observations by the Rosetta mission have shown that for 67/P Churyumov-Gerasimenko, as for 1P/Halley before it, cometary ices are depleted in nitrogen (Filacchione et al. 2019). The COSIMA instrument on board measured an average N/C of 0.035 ± 0.011, which is similar to the ratio found in the insoluble organic matter extracted from carbonaceous chondrite meteorites and in most micrometeorites and interplanetary dust particles (Fray et al. 2017). Comparing this ratio with the N/C value of 0.29 ± 0.12 in the Solar System (Lodders 2010), we see that almost 90% of the nitrogen is missing. Recently, one of the missing reservoirs of nitrogen may have been found in comets; the 3.2 µm absorption band is likely to be due to ammonium salts (Altwegg et al. 2020; Poch et al. 2020), with the spectrum of comet 67/P having the same shape of a laboratory spectrum of ammonium formate mixed with pyrhotite grains. Ammonium salts are semi-volatile materials that desorb at higher temperatures than the more volatile NH_3 and H_2O (Viti et al. 2004), which explains why they may have been missed by the COSIMA instrument. The temperature dependence of the solid-to-gas phase abundance ratio of each one of the reservoirs is fundamental to address the overall N budget. The solid phase abundance of each carrier is more easily quantified after its sublimation.

Indeed, NH_3 is central in ice chemistry (Theulé et al. 2013) as it bears the lone pair of the N atom that favors the nucleophilic addition reaction where CO_2 gives ammonium carbamate $NH_4^+NH_2COO^-$ and carbamic acid NH_2COOH (Bossa et al. 2008; Noble et al. 2014; Potapov et al. 2019), and it acts as the base in acid–base reactions with HNCO (Mispelaer et al. 2012), HCN (Noble et al. 2013), HCOOH (Bergner et al. 2016), and HCl, which gives ammonium cyanate $NH_4^+OCN^-$, ammonium cyanide $NH_4^+CN^-$, ammonium formate $NH_4^+HCOO^-$, and ammonium chloride $NH_4^+Cl^-$ salts, respectively.

The NH_3/NH_4^+ hydride is an important tracer of the chemical evolution of the Solar System as it is detected in the proto-solar nebula, in the Solar System bodies, and in planetary atmospheres (Caselli & Ceccarelli 2012). This is why understanding how and in what chemical form it travels from the primitive molecular cloud until it is incorporated in other bodies is a key question in understanding the complex formation history of the Solar System.

Determining the nitrogen $^{14}N/^{15}N$ or the hydrogen H/D isotopic ratios in different bodies of the Solar System provides important information regarding the Solar System's origin (Caselli & Ceccarelli 2012). The $^{14}N/^{15}N$ ratio varies greatly from body to body in the Solar System (Hily-Blant et al. 2013), from an initial value of 441 (without corrections due to cosmic evolution) in the Solar nebula (Marty 2012) to a value of 272 in the Earth atmosphere (Marty 2012), a value of 140 in comets for all N-bearing species (HCN, CN, NH_2; Rousselot et al. 2014), and values from 5 to 3000 in meteorites (Bonal et al. 2010) enriched in ^{15}N. Similarly, the D/H ratio can vary significantly in different objects in the Solar System, from carbonaceous chondrites to comets or planetary moons (Alexander et al. 2012), and imposes constraints on the extent of their pre-solar heritage. The D/H exchange in ice is dominated by water and by its crystallization, and is more efficient for N-bearing and O-bearing molecules rather than for C-bearing molecules (Faure et al. 2015a,b).

To make these observations meaningful, it is important to retrace the journey of the main N-carriers from the pre-solar nebula (a cold radiation-rich environment, favoring isotopic fractionation) to the Solar System bodies. Although NH_3 and NH_4^+ are the main observed carriers in ice, they account for less than 10 % of the overall nitrogen elemental budget (Öberg et al. 2011); HCN or N_2 are not detected in ices (Boogert et al. 2015). While NH_3 is a volatile species (it desorbs before or with water), NH_4^+ is a refractory species that has been detected in cometary spectra after the water ice has sublimated (Altwegg et al. 2020; Poch et al. 2020). Actually, the incorporation of nitrogen in the (acid) soluble or insoluble matter of chondrites depends on the amount and form of N-bearing molecules inherited from the proto-solar nebula ice (Alexander et al. 2017), and the insoluble organic matter may be an important source of Earth's volatile species.

This is why reliable modeling of disk chemistry is under development (Walsh et al. 2014; Visser et al. 2018; D'Angelo et al. 2019), with the gas to surface exchange, through accretion and desorption, being an important part of the modeling. Although a complete modeling is clearly beyond the scope of this paper, we want to show how different treatments of the ammonia desorption can lead to different conclusions.

In its ammonium form, nitrogen is more refractory (Gálvez et al. 2010) and can be stored on grains in the inner side of the snow line, which corresponds to the water ice mantle desorption. In the form of ammonium, the amount of nitrogen that can be incorporated into the planetesimals and later into primitive planetary atmospheres depends on its desorption mechanisms and is still an open question. Because of the temperature gradient in the protoplanetary disk, because of the migration of protoplanets in the disk, and because this history can be traced through the $^{15}N/^{14}N$ ratio (Caselli & Ceccarelli 2012), the temperature dependence of the location of the different nitrogen carriers, compared to the water and methanol snow lines, is a fundamental step to understand planet formation (Vernazza et al. 2017). To support observations and in situ space missions like the Rosetta mission, it is important to characterize the desorption process of species in addition to their temperature dependent IR spectra. To our knowledge, only the desorption of the ammonium cyanide salt, $NH_4^+CN^-$, has been quantitatively studied to date (Noble et al. 2013).

In this paper, we conducted a laboratory study of the desorption of ammonium formate, $NH_4^+HCOO^-$, and ammonium acetate, $NH_4^+CH_3COO^-$, salts with and without a water ice substrate. We performed temperature-programmed desorption (TPD) experiments to study both the desorption mechanism and the reactivity of the two salts during the desorption process, using an experimental setup mimicking the interstellar conditions. We describe the ultra-high vacuum (UHV) apparatus along with the experimental protocol and data analysis in Sect. 2. In Sect. 3, we present the results of our two complementary techniques, infrared and mass spectroscopy. We discuss the results and try to answer the following questions: what are the binding energies? When are ammonium salts formed and destroyed? Is it the ions or neutrals that mostly desorb? Does the presence of water affect the formation and desorption of salts? In Sect. 4 we discuss the astrophysical implications of ammonium salts desorption, especially in the context of planetary formation.

2. Experimental

All experiments were conducted with the novel multi-beam UHV apparatus called VErs les NoUvelles Synthèses (VENUS) based at the LERMA laboratory at the CY Cergy Paris University. VENUS has been described in detail elsewhere (Congiu et al. 2020) and only a brief account of the most relevant aspects

Table 1. Experiments and corresponding ice composition, thickness, and deposition temperature.

Exp.	Ice composition	Thickness (monolayers)	T_{dep} (K)
i	NH_3	6.5	10
ii	HCOOH	4.5	10
iii	HCOOH : NH_3	3.7 : 4.5	10
iv	HCOOH : NH_3	3.7 : 4.5	120
v	H_2O : HCOOH : NH_3	15 : 3.7 : 4.5	120
vi	CH_3COOH	2.5	120
vii	H_2O : CH_3COOH	15 : 2.5	10
viii	CH_3COOH : NH_3	2.5 : 4.5	120

of the experimental setup is given here. The experiments were carried out under UHV conditions (base pressure 2×10^{-10} hPa at 10 K) in a stainless steel chamber. The sample holder is made of a circular copper mirror coated with gold, and mounted onto the cold head of a closed-cycle He cryostat. The sample temperature can be controlled in the 7–400 K range by using a regulated resistive heater clamped on the back of the sample holder. The ice analogs were prepared from gas condensation of molecular effusive beams aimed at close normal incidence onto the gold substrate or, in specific cases, on a slab of water ice deposited on the sample holder. The evolution of the ice during deposition was monitored by Fourier transform reflection absorption infrared spectroscopy (FT-RAIRS) using a Vertex 70 spectrometer. Once the desired ice thickness of a few layers was reached, the sample was analyzed by means of the TPD technique.

The TPD technique is used to identify the nature of desorbing species by mass and it is also a powerful method for deriving binding energies of molecules adsorbed on surfaces. The method consists in increasing gradually the temperature of the surface at a constant heating rate while registering the desorption signal (a mass spectrum) as a function of sample temperature. VENUS is equipped with a Hiden 51/3F quadrupole mass spectrometer (QMS) placed 5 mm in front of the sample to monitor gas phase species in the UHV chamber.

The desorption characteristics of pure ices and ice mixtures (NH_3:HCOOH and NH_3:CH_3COOH) were investigated. An overview of the performed experiments is reported in Table 1. For the mixtures (Exp. iii, iv, v, vii, viii) the proportion of ammonia was set to be 20% higher, which should favor the reaction with the acid; the same will occur in the ISM conditions since ammonia is an abundant constituent of interstellar ices which correspond to a fraction of a few percent of the ice, whereas acids are thought to be around one percent (Boogert et al. 2015). The heating ramp was set to 0.2 K s^{-1} for all experiments, with each TPD starting from the deposition temperature. In the figures of this paper, the notation $\{sampleA + sampleB\}^{T}_{A:B}$ is used to indicate that the gases were co-deposited at temperature T and the estimated final thickness of each sample is A:B, expressed in monolayers (MLs), where 1 ML = 10^{15} molecules cm^{-2}. As an example, $\{HCOOH + NH3\}^{10\,K}_{3.7:4.5\,ML}$ means that we have co-deposited 3.7 ML of HCOOH and 4.5 ML of NH_3 at 10 K on the gold-coated target. The average H_2O ice coverage in ISM is supposed to be from a sub-monolayer regime up to 30 ML (Potapov et al. 2020), or even to a few hundreds according to some authors. Here, the final thickness of the samples does not exceed 10 ML in the experiments without water and 25 ML in the experiment with water (Exp. v), which is a good approximation to the ISM conditions.

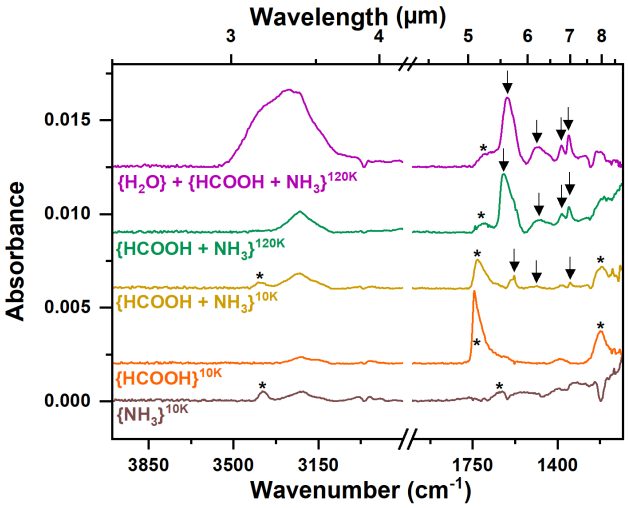

Fig. 1. RAIRS spectra of experiments related to the formation of ammonium formate. The bands highlighted by stars (*) correspond to the absorption features of the neutral molecules NH_3 and HCOOH. When these two species are co-deposited, vibrations of the molecular ions (NH_4^+ and $HCOO^-$) appear (↓), suggesting the formation of ammonium formate.

3. Results

The results of this chapter focus on the desorption properties of ammonium formate and ammonium acetate. To address this point, first the IR and TPD characteristics of pure species, NH_3, HCOOH, and CH_3COOH, are presented. Then, the experiments involving ice mixtures are described, where the IR spectra is used to follow the reaction to produce ammonium salts. Finally, the desorption kinetics parameters of ammonium formate and ammonium acetate were obtained using their TPD spectra and we discuss the desorption behavior of the salts.

3.1. Desorption of ammonium formate

3.1.1. Pure ices: HCOOH and NH_3

The IR spectra of pure NH_3 and HCOOH are shown in Fig. 1. The attributed absorption bands are listed in Table 2. Both spectra were recorded at the end of the deposition of each species carried out at 10 K. The film thickness in all experiments corresponds to a few monolayers (6.5 ML for NH_3 and 4.5,ML for HCOOH); for this reason the IR spectrum recorded is at the limit of the signal-to-noise ratio of the spectrometer. The IR spectrum of solid NH_3 is well documented in the literature (D'Hendecourt & Allamandola 1986; Sandford & Allamandola 1993; Noble et al. 2013; Bouilloud et al. 2015), and here we can distinguish between two important bands: the NH_3 ν_3 and ν_4 modes at 3375 cm^{-1} and 1641 cm^{-1}, respectively. There is also a feature around 3200 cm^{-1} attributed to crystalline water that grows on the window of the IR detector itself, located outside of the experimental chamber. This band is likely to affect the spectrum in its surroundings so extreme care was taken in analyzing features in the vicinity of 3200 cm^{-1} under our experimental conditions.

The IR properties of HCOOH were studied in detail in Bisschop et al. (2007). The formic acid spectrum in Fig. 1 displays two bands at 1743 and 1222 cm^{-1}. The prominent peak at 1743 cm^{-1} originates from the ν(C=O) stretching vibration, while the band at 1222 cm^{-1} is due to the ν(C–O) stretching mode of HCOOH.

Table 2. Infrared band assignments (cm^{-1}) of NH_3, HCOOH, and CH_3COOH as pure ices and as ice mixtures.

Mode	NH_3 (i)	HCOOH (ii)	HCOOH:NH_3 (iii)	(iv)	H_2O:HCOOH:NH_3 (v)	CH_3COOH (vi)	(vii)	CH_3COOH:NH_3 (viii)
NH_3 (ν_4, NH bend)	1641	–	–	–	–	–	–	–
NH_3 (ν_3, NH bend)	3375	–	3380	–	–	–	–	–
HCOOH (ν, C–O st)	–	1222	1216	–	–	–	–	–
HCOOH (ν, C=O st)	–	1743	1730	1710	1697	–	–	–
$HCOO^-$ (ν_4,C–O s-st)	–	–	1346	1353	1353	–	–	–
$HCOO^-$ (δ, CH st)	–	–	1382	–	1384	–	–	–
NH_4^+ (ν_4, NH bend)	–	–	1487	1475	1482	–	–	1500
$HCOO^-$ (ν_2, C–O a-st)	–	–	1579	1621	1608	–	–	–
CH_3COOH (ν, C=O st)	–	–	–	–	–	1724	1716	1700
CH_3COOH (ν, C=O a–st)	–	–	–	–	–	1643	1655	–
CH_3COOH (δ, CH_3 a–st)	–	–	–	–	–	1413	1428	–
CH_3COOH (ν, C–O st)	–	–	–	–	–	1307	1290	1292
CH_3COO^- (ν, C=O st)	–	–	–	–	–	–	–	1575
CH_3COO^- (ν, C=O a-st)	–	–	–	–	–	–	–	1428

References. D'Hendecourt & Allamandola (1986); Sandford & Allamandola (1993); Noble et al. (2013); Bouilloud et al. (2015); Bisschop et al. (2007); Hellebust et al. (2007); Gálvez et al. (2010); Bahr et al. (2006); Ito & Bernstein (1956); Sivaraman et al. (2013).

Figure 2 presents the TPD profiles of the experiments involving HCOOH and NH_3. The left panels, a and c, show the desorption of pure species deposited directly onto the gold substrate. In the case of pure NH_3, in addition to the parent ion NH_3^+, the fragment ion NH_2^+ was also monitored by the quadrupole mass spectrometer. The resulting TPD mass spectrum shows the desorption of the parent molecule (m/z = 17) and the fragment at m/z = 16, with both maxima of desorption peaking at around 94 K. These two mass signals always present a constant ratio of ~2:1. We note that the ratio of fragments depends on the kinetic energy of ionizing electrons, which is set to 30 eV in our spectrometer, thus lower than the typical value of 70 eV. The value of 30 eV was chosen to optimize the stability of the system and reduce fragmentation.

In the interstellar medium a key parameter that governs the chemical abundance in the solid and in the gas phase is the residence time of species on the dust-grain surface determined by their desorption rate. In an out-of-equilibrium treatment desorption from a surface, considering an open volume, the rate of the desorption, $\frac{dN}{dT}$, can be described by the Wigner–Polanyi equation

$$-\frac{dN}{dt} = k_{des} N^n, \quad (1)$$

where k_{des} is the desorption rate constant, N is the number of adsorbed molecules, n is the order of the reaction and the minus sign accounts for the loss of molecules from the surface. For thermal desorption, k_{des} depends on the binding energy of the specific species adsorbed, and is given by the Arrhenius law:

$$-\frac{dN}{dt} = A \exp\left(-\frac{E_{bind}}{RT}\right) N^n. \quad (2)$$

Here, A is a pre-exponential factor, E_{bind} is the binding energy of the species, R is the gas constant and T is the surface temperature. During a TPD experiment the sample is heated at a constant rate $\frac{dT}{dt} = \beta$, and Eq. (2) can be rearranged in terms of the temperature and β to derive the kinetic parameters A and E_{bind} from the experimental data,

$$-\frac{d\theta}{dT} = \frac{A}{\beta} \exp\left(\frac{-E_{bind}}{RT}\right) \theta^n, \quad (3)$$

where $\frac{d\theta}{dT}$ is the desorption rate (ML K^{-1}), A a pre-exponential factor in s^{-1} for a first-order desorption n = 1, θ is the surface coverage in ML, E_{bind} is the binding energy for desorption (J mol^{-1}), R is the gas constant (J K^{-1} mol^{-1}), and T is the temperature of the surface (K).

To obtain the binding energies and pre-exponential factors from the TPD curves from Eq. (3), a standard minimization of χ^2 is used, which reflects the sum of the squares of the differences between the experimental and the calculated profiles (Acharyya et al. 2007). The values of desorption rate as a function of the temperature and the surface coverage were obtained directly from the experimental data. In order to work with only the binding energy as a free parameter during the fit, we used the method proposed by Noble et al. (2013), where the pre-exponential factor value is fixed. We start assuming that the lattice vibrational frequency of the solids is 10^{13} s^{-1}. However, if the number of vibrational modes of the molecule increases, as is the case of molecules with a larger number of atoms, the lattice vibrational frequency also tends to increase and the value of the pre-exponential factor has to be optimized and increased gradually in order to reduce the χ^2 value.

Using this approach, the couple binding energy and pre-exponential factor were estimated assuming a first-order process (n = 1) for pure NH_3: $E_{bind} = 25.5 \pm 0.1$ kJ mol^{-1} and $A = 1.0 \pm 0.2 \times 10^{13}$ s^{-1}. These values are consistent with those obtained from experimental techniques (Ulbricht et al. 2006; Noble et al. 2013; Martín-Doménech et al. 2014) and are reported with our other values in Table 3. It should be noted that these binding energies correspond to the interaction of ammonia with an inert gold surface. Binding energies for NH_3 on interstellar water ice were recently computed by Ferrero et al. (2020).

Panel c of Fig. 2 displays the TPD curve of pure formic acid. Two desorption components, at 138 and 152 K, can be distinguished in the spectra possibly because of the formation of different phases of formic acid with an amorphous and a crystalline structure. The desorption behavior of formic acid was studied previously by Bahr et al. (2005), Hellebust et al. (2007), and recently by Chaabouni et al. (2020). Dimeric HCOOH can be present in the gas phase and remains in this form as an amorphous film during deposition being later

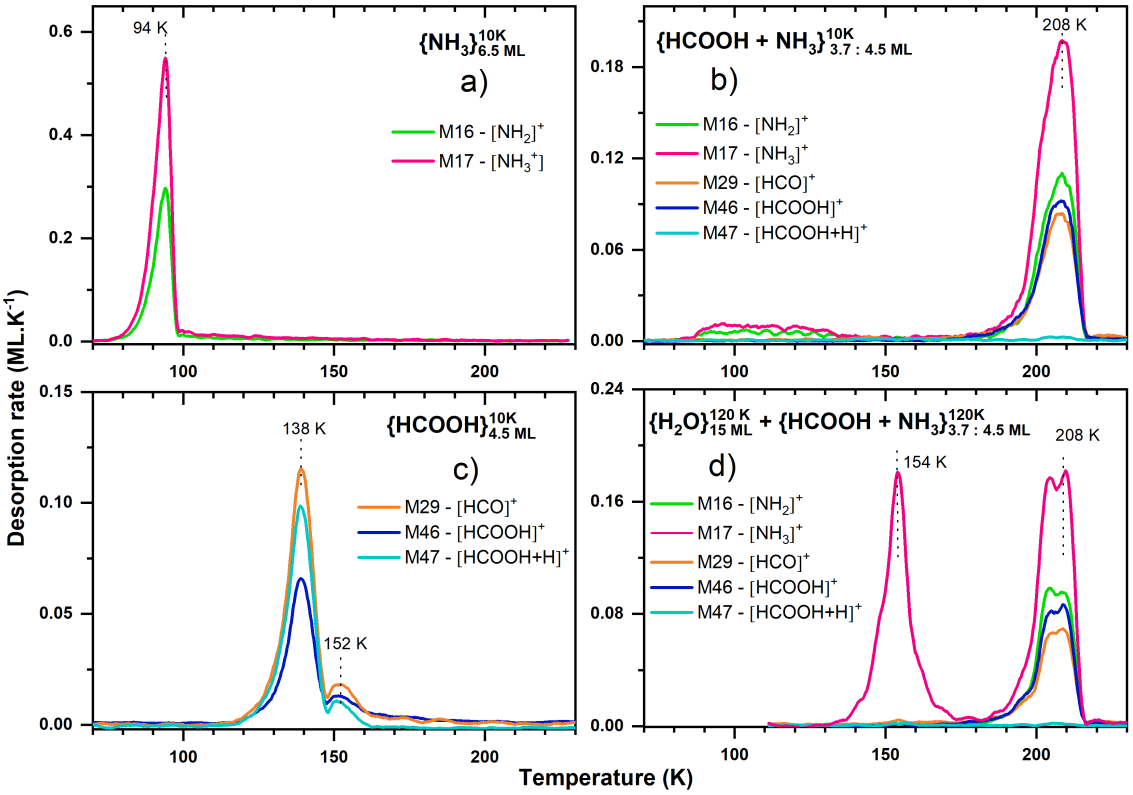

Fig. 2. TPD spectra of experiments involving ammonium formate. *Left panels*: TPD spectra of (a) pure NH_3 and (c) pure HCOOH. *Right panels*: TPD spectra of mixed NH_3 and HCOOH (b) without and (d) with a substrate of water. The desorption component around 208 K traces the desorption of $NH_4^+HCOO^-$; the ratio of its fragments, similar to those of pure molecules, indicates the dissociation of the salt during the desorption process back into the components NH_3 and HCOOH.

Table 3. Kinetic parameters for the desorption of ammonium salts and their neutral components compared with available reference values.

Molecule	E_{bind} (kJ mol^{-1})	A (s^{-1})	Reference
NH_3	25.5 ± 0.1	$1.0 \pm 0.2 \times 10^{13}$	This work
	26 ± 1	$1.0 \pm 0 \times 10^{13}$	Noble et al. (2013)
HCOOH	38.3 ± 0.1	$1.1 \pm 0.2 \times 10^{13}$	This work
	27.8–47.7	1.0×10^{13}	Chaabouni et al. (2020) [(a)]
	27.1–49.1	1.0×10^{13}	Shiozawa et al. (2015) [(a)]
CH_3COOH	46.8 ± 0.2	$1.1 \pm 0.2 \times 10^{13}$	This work
	55 ± 2	$8 \times 10^{17\pm3}$	Burke et al. (2015)
$NH_4^+HCOO^-$	68.9 ± 0.1	$7.7 \pm 0.6 \times 10^{15}$	This work
$NH_4^+CH_3COO^-$	83.0 ± 0.2	$3.0 \pm 0.4 \times 10^{20}$	This work

Notes. Errors arise from the spread of the fit values. [(a)]Values after the conversion with A fixed at 10^{13} s^{-1}.

converted into a crystalline film during annealing (Hellebust et al. 2007).

Formic acid dissociates into several fragments in our experiments, but here only the three major fragments are shown (Fig. 2c). The fragment at $m/z = 46$ is related to the ionized parent molecule $HCOOH^+$, while the fragment of higher intensity in the TPD spectra (at $m/z = 29$) is due to the loss of a hydroxyl group, –OH, a common pattern in carboxylic acids that gives HCO^+ fragments in the case of HCOOH. The fragment at $m/z = 47$ can be attributed to the formation of dimeric formic acid that breaks up resulting in HCOOH-H^+ species (Chaabouni et al. 2020).

The binding energy and the pre-exponential factor derived using Eq. (3) for formic acid are $E_{bind} = 38.3 \pm 0.1$ kJ mol^{-1} and $A = 1.1 \pm 0.2 \times 10^{13}$ s^{-1}. To compare the binding energy value with the previously published results of the kinetic parameters of formic acid, we used the method described in Chaabouni et al. (2018). Since there is a relation between A and E_{bind}, we can use the same pre-exponential factor ($A = 10^{13}$ s^{-1}) and convert the values provided by Shiozawa et al. (2015) and Chaabouni et al. (2020) to compare with our results. From Table 3, we can see that the binding energy values for formic acid found in these different studies are similar, and that under our conditions of thickness and on a gold substrate the values we find are between the values

corresponding to the HCOOH monomer and dimer. This may indicate that in our experiment HCOOH is desorbing from the surface as a mixture of both forms of HCOOH.

3.1.2. Mixed ices: HCOOH + NH_3

To form $NH_4^+HCOO^-$ salt, HCOOH and NH_3 gases were injected into the VENUS main chamber using two separated molecular beams, and co-deposited on the gold surface held at two different temperatures, 10 and 120 K. The flux of the NH_3 beam was set to be 20% higher than the HCOOH beam, which should favor the reaction between the two species.

Figure 1 shows the IR spectra of HCOOH + NH_3 deposited at 10 and 120 K (displayed in yellow and green, respectively). In the experiment conducted at 10 K, it is possible to see absorption features of both species in their neutral form. Comparing this spectrum with the spectra of pure NH_3 and HCOOH, we can distinguish the presence of NH_3 due to the 3380 cm^{-1} absorption band, while in the low wavenumber range two features can be attributed to HCOOH: the high intensity absorption band at 1730 cm^{-1} due to the C=O stretch and the broad band at 1216 cm^{-1} due to C−O stretch. Three other bands can be distinguished in the spectrum, indicated by arrows, and are consistent with the salt bands associated with the formation of ammonium formate ($NH_4^+HCOO^-$). A broad band of low intensity around 1487 cm^{-1} is attributed to the ν_4 NH bending mode of NH_4^+ ions, and two other absorption bands are found related to $HCOO^-$, the ν_4 C−O asymmetric and symmetric stretch at 1579 and 1346 cm^{-1} (Hellebust et al. 2007; Gálvez et al. 2010; Bergner et al. 2016). The presence of ionic features at 10 K indicates that the samples have undergone a reaction during the deposition phase. The proton transfer between HCOOH and NH_3 is an acid–base reaction that produces $NH_4^+HCOO^-$ and is characterized by a low-activation energy that allows the reaction to occur at cryogenic temperatures (Theulé et al. 2013):

$$HCOOH + NH_3 \longrightarrow NH_4^+HCOO^-. \quad (4)$$

In the experiment where the mixture HCOOH + NH_3 was co-deposited at 120 K the IR features related to the ion species are predominant (Fig. 1, green profile). The most intense band is due to the $HCOO^-$ ν_4 C−O symmetrical stretch, which was blue-shifted to 1621 cm^{-1} compared to the spectrum deposited at 10 K. Additionally, the other salt bands present at 10 K become stronger and, in general, red-shifted: the broad band at around 1475 cm^{-1} of the NH_4^+ ν_4 NH bending mode and the ν_4 C−O symmetric stretch at 1353 cm^{-1}. We note that in the 120 K deposition experiment NH_3 molecules cannot stick and accumulate on the surface since their desorption flux is orders of magnitude higher than their accretion flux. Therefore, only ionic forms can be kept on the surface. Despite the short residence time of NH_3 ($1/k_{des}$ = 0.08 s) at 120 K we observe an efficiency of formation of salts equal to one, normalized to the HCOOH partner. This implies that the formation rate is much higher than the desorption rate. Actually, the gradual temperature increase during a TPD favors the reaction between the components producing ammonium formate (Hellebust et al. 2007; Gálvez et al. 2010; Bergner et al. 2016).

The right panels of Fig. 2 display the TPD spectra of experiments involving HCOOH and NH_3 mixtures deposited at 10 K without water (b) and at 120 K with water (d). The fragments displayed in the TPD curves of mixed ices are the same shown for pure species. In the experiment performed at 10 K (Fig. 2b) the desorption occurs in two steps. A first desorption starts at

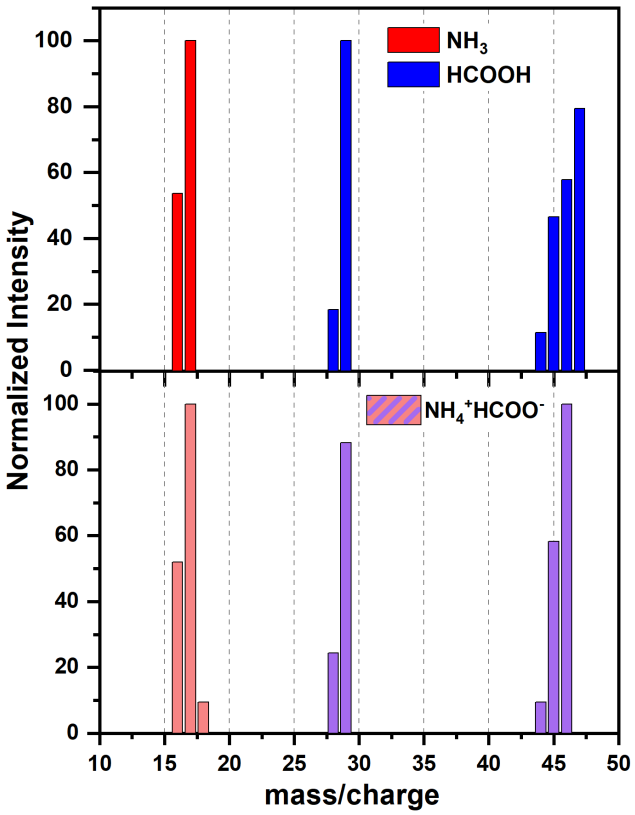

Fig. 3. Mass spectra of NH_3, HCOOH, and $NH_4^+HCOO^-$. Intensities are normalized to the most intense of the peaks for NH_3 (m/z = 17) and HCOOH (m/z = 29). For $NH_4^+HCOO^-$ the fragments corresponding to ammonia are normalized to the most intense of the peaks (m/z = 17) and those from formic acid to the second most intense peak (m/z = 46).

80 K and only fragments m/z = 16 and 17 have a relevant intensity. This peak can be attributed to the desorption of NH_3 in excess, which did not react with HCOOH to produce ammonium formate during the warm-up. The second feature shows the desorption of fragments at m/z = 16, 17, 29, and 46, and occurs at around 208 K. This component desorbing at temperatures higher than the desorption of pure HCOOH and pure NH_3 is attributed to the desorption of ammonium formate. The desorption energy estimated using Eq. (3) for ammonium formate is E_{bind} = 68.9 ± 0.1 kJ mol^{-1} with a pre-exponential factor $A = 7.7 \pm 0.6 \times 10^{15}$. Since the stoichiometry of reaction (4) is 1:1, the reaction yield can be estimated considering the limiting reactant HCOOH consumed during the experiment. No residual formic acid desorbs at high temperature, which suggests that all formic acid available reacted with ammonia to produce ammonium formate. Moreover, the areas of TPD peaks confirm mass conservation of the deposited species, indicating that there was no loss prior to desorption and that no change in detection efficiency of the QMS occurred.

The desorption profile of ammonium formate also indicates that the salt dissociates releasing neutral ammonia and formic acid to the gas phase at temperatures higher than the desorption temperatures of the pure species. This argument is corroborated because the same fragmentation pattern shows up in the mass spectra of pure HCOOH and pure NH_3 and in the TPD spectrum of ammonium formate (Fig. 3). In particular, we observe the exact ratio of mass 17 to mass 16, in addition to the conservation of the total amount deposited. This would have been impossible if a substantial fraction of ammonia had desorbed in

the form of NH_4^+, or directly in the form of salt, which implies a different cracking pattern.

The mechanisms of sublimation of ammonium salts were investigated through $NH_4^+Cl^-$ systems by Zhu et al. (2007). The study found that the rate-controlling step in the dissociation of $NH_4^+Cl^-$ salt is the formation and desorption of the $[NH_3 \cdots HCl]$ complex that later dissociates without a distinct barrier into $NH_{3(g)}$ and $HCl_{(g)}$. Although in our experiment we cannot measure the formation of a $[NH_3 \cdots HCOOH]$ complex, we observe that the salt dissociates and releases the neutral components into the gas phase:

$$NH_4^+ HCOO^-_{(s)} \rightleftharpoons NH_{3(g)} + HCOOH_{(g)}. \quad (5)$$

In addition, only the fragment at $m/z = 47$ that is associated with the cracking pattern of HCOOH dimers is absent in the TPD spectrum of ammonium formate, suggesting that formic acid does not re-associate into its dimeric form in the gas-phase before reaching the QMS.

3.1.3. Influence of water ice mantles on the desorption of ammonium salts

The experiment involving the $HCOOH + NH_3$ mixture in the presence of water carried out at 120 K allows us to evaluate the effects of water ice mantles on the desorption of ammonium salts. The RAIRS spectrum of this experiment does not show a significant difference in absorption features in the spectral interval between 2000 cm^{-1} and 1100 cm^{-1}. The main difference is seen at around 3000 cm^{-1} and shows the characteristic broad band of water due to the $-OH$ stretch.

Panel d of Fig. 2 shows the desorption rate of ammonium formate on a water ice substrate deposited at 120 K. At around 154 K water desorption reaches its maximum, as we can see from the ion at $m/z = 17$, which is 14% of that at $m/z = 18$ (not shown for clarity). The second desorption peak at around 208 K exhibits the same characteristics as the mass spectra recorded in experiments performed on the bare gold target from 10 or 120 K. The water substrate does not influence the TPD profiles of $NH_4^+HCOO^-$, and the salt desorbs as a semi-volatile species after complete desorption of the water ice substrate.

3.2. Formation and desorption of ammonium acetate

3.2.1. Pure CH_3COOH

The IR spectra of pure acetic acid deposited at 10 and 120 K are displayed in Fig. 4. The influence of the deposition temperature and the effect of two substrates (gold and water ice) were evaluated. In the presence of water, acetic acid deposited at 10 K displays three IR bands at low frequencies assigned to the vibration of the carbonyl group. Two bands related to the $\nu(C=O)$ absorption feature at 1716 cm^{-1} and 1655 cm^{-1} are observed convoluted. These bands and the absorption at 1290 cm^{-1} are attributed to acetic acid dimers following the values reported in previous studies (Bahr et al. 2005; Hellebust et al. 2007). When the deposition temperature increases from 10 to 120 K the bands become narrower and resolved. The 1643 cm^{-1} feature has a broad absorption and low intensity, while the 1722 cm^{-1} and 1290 cm^{-1} bands are sharper and the most intense bands over the spectra.

The upper panel in Fig. 5 shows the desorption profile of CH_3COOH and NH_3 for comparison, already discussed in the previous section. Acetic acid breaks up into several species, the most intense fragment corresponding to $m/z = 43$, and is attributed to CH_3CO^+ generated after the loss of its hydroxyl group. The fragments related to the parent molecule CH_3COOH^+ and the dimer $CH_3COOH-H^+$ are the traces for $m/z = 60$ and 61.

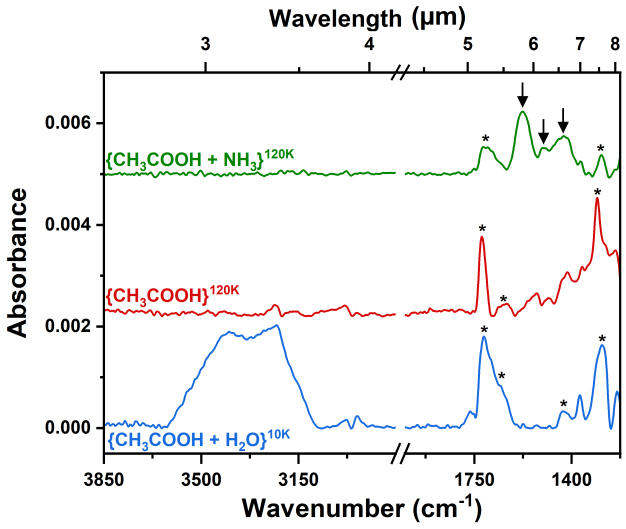

Fig. 4. RAIRS spectra of experiments involving the formation of ammonium acetate. The highlighted bands using stars are related to absorption features of neutral acetic acid. When NH_3 and CH_3COOH are co-deposited, the bands related to $NH_4^+CH_3COO^-$ appear (indicated by arrows.)

The calculated values of binding energy and pre-exponential factor for the desorption of acetic acid are $E_{bind} = 46.8 \pm 0.2$ kJ mol^{-1} and a pre-exponential factor $A = 1.1 \pm 0.2 \times 10^{13}$ s^{-1}, which are in a good agreement with the values reported previously in the literature (Burke et al. 2015).

3.2.2. Mixed ices: CH_3COOH + NH_3

The IR spectrum of the $CH_3COOH + NH_3$ mixture deposited at 120 K is shown in Fig. 4. To our knowledge, the IR spectrum of ammonium acetate has never been reported in the literature, so we used the IR bands of sodium acetate and methyl acetate to identify the salt features (Ito & Bernstein 1956; Sivaraman et al. 2013). The $\nu(C=O)$ asymmetrical and symmetrical stretch at 1575 and 1428 cm^{-1} are attributed to CH_3COO^- ions. The IR spectrum of sodium and methyl acetate do not display any prominent absorbance in the range between 1490 and 1600 cm^{-1}, hence we attribute the 1500 cm^{-1} absorbance to the $\nu(N-H)$ bending mode of NH_4^+, corresponding to the same pattern seen in the spectrum of ammonium formate.

The bottom panel of Fig. 5 presents the TPD profile of the $CH_3COOH + NH_3$ mixture deposited at 120 K. The spectra do not display traces of ammonia or acetic acid desorbing as pure species at temperatures below 180 K. The desorption peak at around 200 K is attributed to the desorption of ammonium acetate. As discussed for the TPD spectra of ammonium formate, the fragments highlighted are the same as shown for pure acetic acid and ammonia, and indicate that the salt dissociates releasing the base and the acid in their neutral form into the gas phase before being detected by the QMS. In the case of ammonium acetate, the fragment at $m/z = 61$, corresponding to one of the fragments of the CH_3COOH dimers, presents a significant desorption rate, which indicates that dimeric acetic acid could form after the dissociation of the salt.

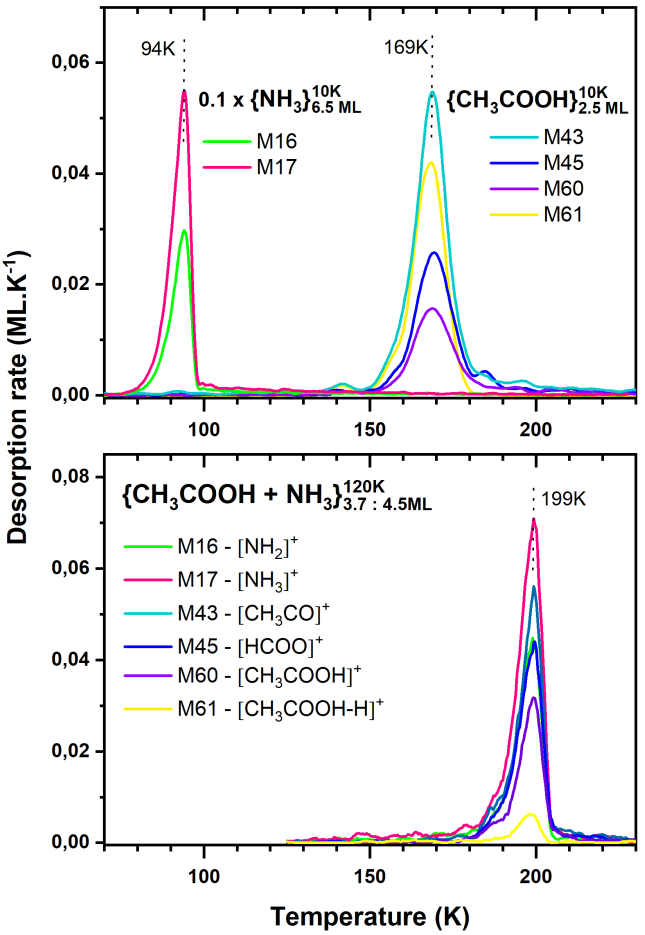

Fig. 5. TPD spectra of experiments involving ammonium acetate. *Top panel*: TPD spectra of NH_3 and CH_3COOH. *Bottom panel*: TPD spectrum of $NH_4{}^+CH_3COO^-$; the sharp profile of the desorption is linked with a high pre-exponential factor and may indicate that the dissociation of the salt is at the origin of the desorption process.

The binding energy for ammonium acetate is estimated to be $E_{\rm des} = 83.0 \pm 0.2$ kJ mol^{-1} with a pre-exponential factor $A = 3.0 \pm 0.4 \times 10^{20}$ s^{-1}. The high value of the pre-exponential factor is a classical trend observed when molecular complexity increases (Tait et al. 2005). Quite astonishingly, it is observed that the desorption of ammonium acetate occurs before that of ammonium formate. Usually, the larger the molecular complexes, the greater the energy of their interaction with the surface, simply because the multiplicity of their interaction increases. This is observed, for example, in the TPD of pure formic and acetic acids, although it is a general rule of thumb (e.g., methanol has a lower binding energy than ethanol, which is lower than that of propanol). This is not what is observed for the salts, and it probably indicates that the desorption of salts occurs concurrently with dissociation into their neutral components. The binding energy would be a kind of measure of the intrinsic stability of the salt, so ammonium formate is more stable than ammonium acetate, which is probably also related to the stronger acidity character of formic acid with respect to acetic acid, and therefore to its greater propensity to donate a proton. The ability to transfer the proton in the forward or backward reaction is translated in the logarithm of the acidity constant (pK_a) of the species. This proves that what we are actually measuring is the activation energy of the endothermic backward reaction

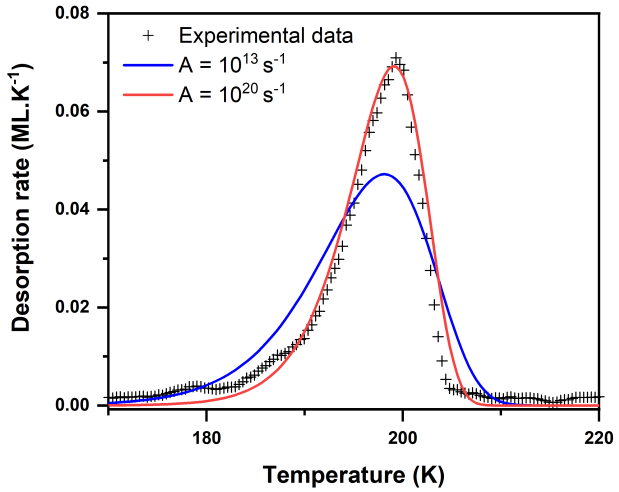

Fig. 6. TPD curve of ammonium acetate is better fitted using a high value of the pre-exponential factor, $A = 10^{20}$ s^{-1}, instead of $A = 10^{13}$ s^{-1} used for the other molecules. This difference probably occurs because we measure the desorption process and a multi-step reaction that includes the dissociation of ammonium acetate.

rather than the desorption energy:

$$NH_4{}^+ CH_3COO^-{}_{(s)} \rightleftharpoons [NH_3 \cdots CH_3COOH]_{(s)}. \quad (6)$$

Once the backward reaction has occurred, the neutrals, which should have desorbed long before (at 199 K $t_{\rm res} = 4.9 \times 10^{-7}$ s for NH_3 and $t_{\rm res} = 1.13$ ms for HCOOH), desorb very rapidly at this range of temperature:

$$[NH_3 \cdots CH_3COOH]_{(s)} \rightleftharpoons [NH_3 \cdots CH_3COOH]_{(g)}, \quad (7)$$

$$[NH_3 \cdots CH_3COOH]_{(g)} \rightleftharpoons NH_{3(g)} + CH_3COOH_{(g)}. \quad (8)$$

The pre-exponential factor hides several physical mechanisms, such as a multi-step desorption composed of several elementary activated processes or a multi-site diffusion energy, resulting in a high (and sometimes temperature-dependent) value of factor A. Figure 6 shows the tentative fit of the acetate TPD trace using a pre-exponential factor $A = 10^{13}$ s^{-1} used for the other molecules, and the best fit obtained using $A = 10^{20}$ s^{-1}. We are measuring a (likely multi-step) chemical reaction rather than a molecular desorption, which can explain the high value of the calculated pre-exponential factor.

4. Discussion

Observations of the N-bearing carriers (the NH_3/NH_4^+ hydride, the nitrogen $^{14}N/^{15}N$ or the hydrogen H/D isotopic ratios in N-bearing hydrides) give information on the chemical evolution of the Solar System, from the proto-solar nebula to the Solar System bodies and/or planetary atmospheres (Caselli & Ceccarelli 2012). Thus, it is important to retrace the chemical journey of the main N-carriers from the pre-solar nebula to the Solar System bodies. NH_3 and NH_4^+ are the main observed carriers in ice, although they account for less than 10% of the overall nitrogen elemental budget (Öberg et al. 2011). These two species behave differently with respect to the desorption.

According to the Viti et al. (2004) classification, NH_3 is a H_2O-like molecule, whose desorption is mostly co-desorption with water ice, and as such it can be modeled following the same

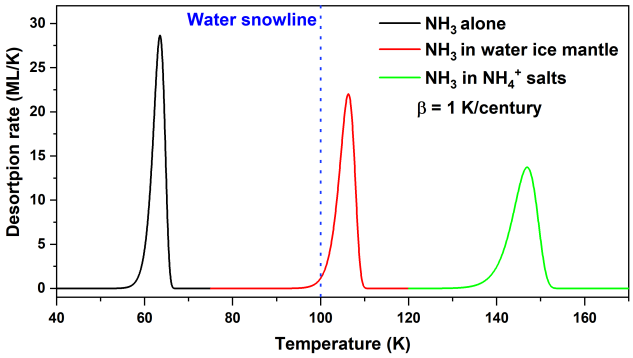

Fig. 7. TPD simulation showing that ammonia can desorb in more than one temperature range depending on its chemical nature and chemical environment. If ammonia is locked in ammonium salts, it desorbs at higher temperature with respect to the water snow line. The heating rate of this simulation is β = 1 K/century, a typical estimation for high-mass stars (Viti & Williams 1999; Viti et al. 2004). For low-mass stars, the heating rate would be slower and the effect of delay even more pronounced.

pattern as the desorption of the water ice mantle. NH_4^+ is a semi-volatile and refractory species (the term refractory applying to species incorporated in the dust grain by a covalent bond and sublimating at much higher temperatures than that of water ice), and the characteristics of its desorption have been measured in this paper. NH_3 can be easily converted into NH_4^+ by a set of thermal reactions involving proton transfer (Theulé et al. 2013) in the temperature range found in the warm layers of the disk or even in the disk mid-plane for a low-mass protostar, or in any region of the disk in the case of a high-mass protostar.

We consider three scenarios: (i) the desorption of NH_3 ($A = 1.0 \times 10^{13}$ s^{-1}, E = 25.5 kJ mol^{-1}) desorbing from a surface as a pure species; (ii) complete co-desorption of NH_3/NH_4^+ with amorphous water ice ($A = 10^{18}$ s^{-1}, E = 54.5 kJ mol^{-1}) that coincides with desorption from the water snow line location in the disk; and (iii) delayed desorption of NH_4^+ ($A = 7.7 \times 10^{15}$ s^{-1}, E = 68.9 kJ mol^{-1}, calculated in this work) corresponding to desorption from an ammonium line. We can see in Fig. 7 that, depending on the parameters used in the ammonia and/or ammonium desorption, the amount of nitrogen stored in Solar System bodies located beyond the snow line can be considerably different, and can have implications for the formation of the Solar System. Since ammonia is the only base, many species present in the ice can undergo either an acid–base reaction or a nucleophilic reaction with it (Theulé et al. 2013). As a result, most of the NH_3 present in the ice should be locked in a more complex species such as an ammonium salt, which implies a delayed desorption with respect to pure NH_3.

Another important aspect lies in the mild temperature chemistry of semi-volatile species. While the chemistry of the parent molecules (NH_3, HNCO, HCOOH, CO_2) have been extensively studied either under conditions present in molecular clouds or during the warming resulting from a star formation process (Raunier et al. 2004; Bossa et al. 2008; Bertin et al. 2009; Bergner et al. 2016), the chemistry of their products, the salts, have not been studied to a significant extent under conditions present beyond the snow line. Indeed, all molecules present in the icy mantles were supposed to co-desorb with water at the snow line or at lower temperatures if considered volatile species. The presence of semi-volatile species beyond the snow line, at distances smaller than about 3 AU from the protostar, enables three processes: (i) a mild thermal chemistry (around 200 K); (ii) a dry (water-free) photo-chemistry; and (iii) a dry ion or electron-induced chemistry due to the solar winds. Since these three energetic processes are stronger beyond the snow line, semi-volatile molecules are more likely to be included in the soluble or insoluble matter of meteorites. As an example, ammonium perchlorate salt $NH_4^+ClO_4^-$ produces hydroxylamine NH_2OH upon electron radiolysis (Góbi et al. 2017).

An interesting finding of this work is that most of the NH_4^+ is converted into NH_3 by a back transfer of the proton during the desorption processes, and consequently the activation barrier of the thermal reaction $NH_4^+HCOO^- \rightarrow NH_2CHO + H_2O$ (Lorin et al. 1864) is too high to produce formamide in detectable amounts. Historically, this is how formamide was produced industrially from the heating of ammonium formate (Lorin et al. 1864). In a forthcoming paper we will address the reactivity of salts upon H-atom bombardment.

5. Conclusion

In this work, we presented an experimental study of the desorption of two ammonium salts, ammonium formate, $NH_4^+HCOO^-$, and ammonium acetate, $NH_4^+CH_3COO^-$, in an astrophysically relevant environment. Based on our results, we conclude the following:

- Using IR spectra of mixtures containing NH_3 and an organic acid, HCOOH or CH_3COOH, we showed that ammonium salts are efficiently produced at temperatures as low as 10 K. They undergo a complete reaction with the increase in temperature, in the presence of water or not, which does not affect the desorption process under our experimental conditions;
- For both salts the ammonium NH_4^+ transfers its proton to the corresponding anion to release ammonia and the corresponding acid (HCOOH and CH_3COOH). No complex organic molecules (e.g., formamide, acetamide, urea) are formed during the desorption process. Ammonia is the only N-bearing species that sublimates so nitrogen atoms return to the gas phase locked in ammonia at temperatures higher than that of desorption of water ice;
- Desorption of ammonium salts follows a first-order Wigner-Polanyi law. The kinetic parameters of the desorption of ammonium salts were examined. Both $NH_4^+HCOO^-$ and $NH_4^+CH_3COO^-$ desorb following a first-order desorption with rate constant $k_{des} = 7.7 \pm 0.6 \times 10^{15} \times \exp(-68.9 \pm 0.1/RT)$ for $NH_4^+HCOO^-$, and $k_{des} = 3.0 \pm 0.4 \times 10^{20} \times \exp(-83.0 \pm 0.2/RT)$ for $NH_4^+CH_3COO^-$. Both salts are semi-volatile species as they desorb at temperatures higher than that of the desorption of water ice, although lower than room temperature;
- In a mixture of water ice and ammonium salt, where the salt constitutes a small percentage of the total, the fraction of $NH_4^+HCOO^-$ that desorbs after the water ice mantle is 98.5% ± 0.5. This high yield shows that a large amount of nitrogen is released after the water ice has completely desorbed.

As we have seen in this study, it is fundamental to consider the chemical nature of the N-bearing molecules to correctly model their desorption in astrophysical environments. The ammonium sublimation zone turns out to be closer to the protostar with respect to the water snow line. This has important implications with regard to the nitrogen reservoir available across the protoplanetary disk.

Acknowledgements. The authors dedicate this paper in celebration of Stephan Schlemmer's 60th birthday on September 7, 2020. We thank him for all his contributions to the field of Laboratory Astrophysics. This project has received funding from the European Union's Horizon 2020 research and innovation programme under the Marie Skłodowska-Curie grant agreement No 811312 for the project "Astro-Chemical Origins" (ACO). It was also supported by the Programme National "Physique et Chimie du Milieu Interstellaire" (PCMI) of CNRS/INSU with INC/INP co-funded by CEA and CNES; the DIM ACAV+, a funding program of the Region Ile de France, and by the ANR SIRC project (GrantANRSPV202448 2020–2024).

References

Acharyya, K., Fuchs, G. W., Fraser, H. J., van Dishoeck, E. F., & Linnartz, H. 2007, A&A, 466, 1005
Alexander, C., Cody, G., Gregorio], B. D., Nittler, L., & Stroud, R. 2017, Geochemistry, 77, 227
Alexander, C. M. O., Bowden, R., Fogel, M. L., et al. 2012, Science, 337, 721
Altwegg, K., Balsiger, H., Hänni, N., et al. 2020, Nat. Astron., 3
Bahr, S., Borodin, A., Höfft, O., Kempter, V., & Allouche, A. 2005, J. Chem. Phys., 122, 234704
Bahr, S., Borodin, A., Höfft, O., et al. 2006, J. Phys. Chem. B, 110, 8649
Bergner, J. B., Öberg, K. I., Rajappan, M., & Fayolle, E. C. 2016, ApJ, 829, 85
Bertin, M., Martin, I., Duvernay, F., et al. 2009, Phys. Chem. Chem. Phys., 11, 1838
Bisschop, S. E., Fuchs, G. W., van Dishoeck, E. F., & Linnartz, H. 2007, A&A, 474, 1061
Bonal, L., Huss, G. R., Krot, A. N., et al. 2010, Geochim. Cosmochim. Acta, 74, 6590
Boogert, A. C. A., Gerakines, P. A., & Whittet, D. C. B. 2015, ARA&A, 53, 541
Bossa, J. B., Theulé, P., Duvernay, F., Borget, F., & Chiavassa, T. 2008, A&A, 492, 719
Bouilloud, M., Fray, N., Bénilan, Y., et al. 2015, MNRAS, 451, 2145
Burke, D. J., Puletti, F., Woods, P. M., et al. 2015, J. Phys. Chem. A, 119, 6837
Caffau, E., Maiorca, E., Bonifacio, P., et al. 2009, A&A, 498, 877
Caselli, P., & Ceccarelli, C. 2012, A&ARv, 20, 56
Caselli, P., Bizzocchi, L., Keto, E., et al. 2017, A&A, 603, L1
Chaabouni, H., Diana, S., Nguyen, T., & Dulieu, F. 2018, A&A, 612, A47
Chaabouni, H., Baouche, S., Diana, S., & Minissale, M. 2020, A&A, 636, A4
Congiu, E., Sow, A., Nguyen, T., Baouche, S., & Dulieu, F. 2020, Rev. Sci. Inst., 91, 124504
D'Angelo, M., Cazaux, S., Kamp, I., Thi, W. F., & Woitke, P. 2019, A&A, 622, A208
D'Hendecourt, L. B., & Allamandola, L. J. 1986, A&AS, 64, 453
Faure, A., Faure, M., Theulé, P., Quirico, E., & Schmitt, B. 2015a, A&A, 584, A98
Faure, M., Quirico, E., Faure, A., et al. 2015b, Icarus, 261, 14
Ferrero, S., Zamirri, L., Ceccarelli, C., et al. 2020, ApJ, 904, 11
Filacchione, G., Groussin, O., Herny, C., et al. 2019, Space Sci. Rev., 215, 19
Fray, N., Bardyn, A., Cottin, H., et al. 2017, MNRAS, 469, S506
Gálvez, O., Maté, B., Herrero, V. J., & Escribano, R. 2010, ApJ, 724, 539
Grevesse, N., Asplund, M., Sauval, A. J., & Scott, P. 2010, Ap&SS, 328, 179
Góbi, S., Bergantini, A., Turner, A. M., & Kaiser, R. I. 2017, J. Phys. Chem. A, 121, 3879
Hellebust, S., O'Riordan, B., & Sodeau, J. 2007, J. Chem. Phys., 126, 084702
Hily-Blant, P., Walmsley, M., Pineau Des Forêts, G., & Flower, D. 2010, A&A, 513, A41
Hily-Blant, P., Bonal, L., Faure, A., & Quirico, E. 2013, Icarus, 223, 582
Ito, K., & Bernstein, H. J. 1956, Rev. Can. Chim., 34, 170
Knauth, D. C., Andersson, B. G., McCandliss, S. R., & Warren Moos H. 2004, Nature, 429, 636
Lodders, K. 2010, in Principles and Perspectives in Cosmochemistry, eds. A. Goswami, & B. E. Reddy (Berlin, Heidelberg: Springer Berlin Heidelberg), 379–417
Lorin, A. & al. 1864, Chem. News J. Phys. Sci., IX, 291
Maiolino, R., & Mannucci, F. 2019, A&ARv, 27, 3
Maret, S., Bergin, E. A., & Lada, C. J. 2006, Nature, 442, 425
Martín-Doménech, R., Muñoz Caro, G. M., Bueno, J., & Goesmann, F. 2014, A&A, 564, A8
Marty, B. 2012, Earth Planet. Sci. Lett., 313, 56
Mispelaer, F., Theule, P., Duvernay, F., Roubin, P., & Chiavassa, T. 2012, A&A, 540, A40
Nieva, M. F., & Przybilla, N. 2012, A&A, 539, A143
Noble, J. A., Theule, P., Borget, F., et al. 2013, MNRAS, 428, 3262
Noble, J. A., Theule, P., Duvernay, F., et al. 2014, Phys. Chem. Chem. Phys., 16, 23604
Öberg, K. I., Boogert, A. C. A., Pontoppidan, K. M., et al. 2011, ApJ, 740, 109
Omont, A. 2007, Rep. Prog. Phys., 70, 1099
Poch, O., Istiqomah, I., Quirico, E., et al. 2020, Science, 367, aaw7462
Potapov, A., Theulé, P., Jäger, C., & Henning, T. 2019, ApJ, 878, L20
Potapov, A., Jäger, C., & Henning, T. 2020, Phys. Rev. Lett., 124, 221103
Punanova, A., Caselli, P., Pineda, J. E., et al. 2018, A&A, 617, A27
Raunier, S., Chiavassa, T., Duvernay, F., et al. 2004, A&A, 416, 165
Riaz, B., Thi, W. F., & Caselli, P. 2018, MNRAS, 481, 4662
Rousselot, P., Pirali, O., Jehin, E., et al. 2014, ApJ, 780, L17
Sandford, S. A., & Allamandola, L. J. 1993, ApJ, 417, 815
Savage, B. D., & Sembach, K. R. 1996, ARA&A, 34, 279
Shiozawa, Y., Koitaya, T., Mukai, K., Yoshimoto, S., & Yoshinobu, J. 2015, J. Chem. Phys., 143, 234707
Sivaraman, B., Nair, B. G., Lo, J. I., et al. 2013, ApJ, 778, 157
Tafalla, M., Santiago-García, J., Hacar, A., & Bachiller, R. 2010, A&A, 522, A91
Tait, S. L., Dohnálek, Z., Campbell, C. T., & Kay, B. D. 2005, J. Chem. Phys., 122, 164708
Theulé, P., Duvernay, F., Danger, G., et al. 2013, Adv. Space Res., 52, 1567
Ulbricht, H., Zacharia, R., Cindir, N., & Hertel, T. 2006, Carbon, 44, 2931
Vernazza, P., Castillo-Rogez, J., Beck, P., et al. 2017, AJ, 153, 72
Vila-Costas, M. B., & Edmunds, M. G. 1993, MNRAS, 265, 199
Visser, R., Bruderer, S., Cazzoletti, P., et al. 2018, A&A, 615, A75
Viti, S., & Williams, D. A. 1999, MNRAS, 305, 755
Viti, S., Collings, M. P., Dever, J. W., McCoustra, M. R. S., & Williams, D. A. 2004, MNRAS, 354, 1141
Walsh, C., Millar, T. J., Nomura, H., et al. 2014, A&A, 563, A33
Zhu, R. S., Wang, J. H., & Lin, M. C. 2007, J. Phys. Chem. C, 111, 13831